Scientific Journal of Impact Factor (SJIF): 4.72

e-ISSN : 2348-4470
p-ISSN : 2348-6406

International Journal of Advance Engineering and Research Development

National Conference On Nanomaterials, (NCN-2017)

Volume 4, Special Issue 6, Dec.-2017 (UGC Approved)

Structural and electrical properties of low temperature fire Mn-Zn nano ferrite for high frequency application

Pankaj Choudhary[1*], A. Yadav[1,2], P. Saxena[1], A. K. Sinha[3] and Dinesh Varshney[1*]

[1]*School of Physics, Vigyan Bhavan, Devi Ahilya University, Khandwa Road Campus, Indore, 452001, India.*
[2]*Department of Physics, Medi-Caps University, Pigdamber, Indore 453331, India.*
[3]*Indus Synchrotron Utilization Division, Raja Ramanna Centre for Advanced Technology, Indore- 452013, India.*

Abstract: *Mn-Zn nano ferrites were synthesized with citric acid as a capping agent by sol gel auto combustion method. Synchrotron and laboratory x-ray diffraction confirms that mixed nano ferrites is crystalline in nature and indexed in cubic crystal structure (space group Fd3m). Reduced crystallite size is obtained from Synchrotron (15.4 ± 0.0001 nm) as compared to laboratory (16 ± 0.001 nm) source. Raman spectroscopy reveals a doublet like nature of A_{1g} mode for Mn-Zn nano ferrites. Dielectric constant (ε') and loss (tan δ) measured in the frequency range from 100 Hz to 10 MHz at different temperature are found to be decreasing along increase in frequency. The ac electrical conductivity of about 0.108 Sm^{-1} at 573 K is observed for Mn-Zn nano ferrites. Frequency dependent dielectric response supports the dielectric polarization and electrical conduction mechanism. Minimum dielectric loss (~ 0.08) [300 K] at 10 MHz showed that synthesized Mn-Zn nano ferrites are desirable for high frequency applications.*

Keywords: *Ferrites, Synchrotron x-ray diffraction, Raman, Dielectric properties.*

1 Introduction

Nanosized ferrites exhibit novel magnetic and dielectric features rich for high frequency applications such as information technology, biological applications, microwave devices, radar circuits, spintronics and biotechnology [1]. Among ferrites, Mn-Zn based nano ferrites are excellent soft magnetic materials in high-frequency devices due to their low loss of eddy current, magnetic resonance imaging (MRI), high Curie temperature and high initial magnetic permeability, which have been studied extensively for office automation, remote monitoring, computers, communications and industrial automation technology [2].

The transition metal cations (Fe^{3+}, Mn^{2+} and Zn^{2+}) in cubic Mn-Zn nano ferrites occupy both tetrahedral sites (A-site) and octahedral sites (B-site). In spinel structure of $ZnFe_2O_4$, all Fe^{3+} ions are at octahedral (B-site) sites and Zn^{2+} ions are at tetrahedral (A-site) site. While to that, $MnFe_2O_4$ with the random distribution of Mn^{2+} ions on both octahedral and tetrahedral sites possesses inverse spinel structure [3]. Hence, Mn-Zn nano ferrites are viewed as a composite soft magnetic material with a mixed structure.

Properties of ferrites are sensitive to their processing conditions such as temperature, composition and microstructure. Ferrites nanoparticles showed unique dielectric properties. Usually, high performance devices require low dielectric loss (tan δ). Lower the tan δ, the higher the efficiency and lower the noise [4]. Keeping this in mind, herein we aimed at synthesizing and characterizing mixed Mn-Zn nanosized ferrites via low temperature synthesis technique. We further report the consistency of evolution of crystal structure, phonon modes and dielectric properties at different temperatures.

2 Experimental Details

The sol-gel auto combustion method is used here for synthesis of $Mn_{0.5}Zn_{0.5}Fe_2O_4$ nano ferrites [5]. The starting materials in their stoichiometry as ($Mn(NO_3)_2$), ($Zn(NO_3)_2{\cdot}6H_2O$) and ($Fe(NO_3)_3{\cdot}9H_2O$) were dissolved in a distilled water. The molar ratio of citric acid to total moles of metal nitrate ions is adjusted at 1:2. The ammonia solution is added to mixed solution to neutralize with a pH ~ 10. The neutralized solution is evaporated to dryness by heating at 120 °C on a hot plate with continuous stirring, until it becomes viscous and finally formed a very viscous gel. The dried gel burnt completely in a self-propagating combustion manner to form a loose powder. The burnt powder was calcined in air at temperature of 800 °C for 8 hour to obtain spinel phase. The powders were pressed into pellets of size 10 mm (diameter) and 1 mm (thickness) by applying a pressure of 8 Tons. The pellets were sintered at 800 °C for 8 h.

The room temperature Lab x–ray diffraction (XRD) was performed using Cu kα_1 radiation (λ = 1.5406 Å) with Bruker D8 advance x-ray powder diffractometer. Also, the Synchrotron x-ray powder diffraction (SXRD) [λ = 0.8042 Å] has been performed on the angle dispersive x-ray diffraction (ADXRD) beamline (BL-12) at Indus-2 synchrotron source (2.5 GeV), India. The Wayne Kerr impedance analyzer 6500B is used in the frequency range of 20 Hz to 120 MHz, *ac*

voltage range from 10 mV to 1 V and temperature range varies upto 1000 °C. The high purity silver conducting paste-coated pellets of Mn-Zn nano ferrites were used for improved electrical contact for dielectric measurement

3 Result and Discussion

The typical Lab x-ray diffraction (XRD) and Synchrotron x-ray diffraction (SXRD) pattern of $Mn_{0.5}Zn_{0.5}Fe_2O_4$ nano ferrites sintered at 800 °C are shown in Fig. 1. It indicates that the diffraction pattern of Mn–Zn nano ferrites is at (111), (220), (311), (400), (422), (511), (440) planes in accordance with the JCPDS standard card no. (22-1012). It also can be seen that the appearance of secondary phase of α-Fe_2O_3 marked with asterisk (*) accompanying with the Mn-Zn ferrite phase, which is obvious in sol–gel combustion synthesis method. With enhance content of Zn^{2+} in Mn-Zn nano ferrites the secondary phase of α-Fe_2O_3 tends to increase consistent with earlier reported data [6, 7].

Synchrotron and lab x-ray diffraction confirms that mixed Mn-Zn nano ferrites form face centred cubic structure with F*d*3*m* space group. The crystallite size is evaluated using Scherer's equation. Decreasing crystallite size of about 15.4 ± 0.0001 nm is obtained from Synchrotron high-energy source and of 16 ± 0.001 nm from low energy laboratory source. Lab XRD is rather noisy and is not fit perfectly. On the other hand, SXRD allows us to select appropriate 2θ with a perfect fitted to yield value of full width half maximum (FWHM). Structural parameters calculated from Lab and Synchrotron XRD as represented in Table 1.

Raman spectra of $Mn_{0.5}Zn_{0.5}Fe_2O_4$ nano ferrites in the frequency range of 200-800 cm^{-1} at 300 K are shown in Fig. 2. Lorentzian line shape was used to fit the Raman spectra and thick smooth lines are fits to the Lorentzian function. The resolved optical phonon modes in Mn-Zn nano ferrites showed a normal mixed spinel structure with space group O_h^7 (*Fd*3*m*). The full unit cell involve 56 atoms but the littlest Bravais cell contains only 14 atoms, which gives rise to 42 normal modes at the Brillouin zone center. Group theory predicts the following modes belonging to the distribution $\Gamma = A_{1g} + E_g + F_{1g} + 3F_{2g} + 2A_{2u} + 2E_u + 4F_{1u} + 2F_{2u}$ where, five fundamental modes are Raman active ($A_{1g} + E_g + 3F_{2g}$) composed to cation – anion distribution of tetrahedral and octahedral sites and four are IR active ($4F_{1u}$). The rest of modes are both Raman (F_{1g}) and IR ($2A_{2u} + 2E_u + 2F_{2u}$) inactive modes [8].

Observed high intense Raman active modes $F_{2g}(1)$ (227.07 cm^{-1}), E_g (294.27 cm^{-1}), $F_{2g}(2)$ (410.36 cm^{-1}), $F_{2g}(3)$ (498.62 cm^{-1}), $A_{1g}(1)$ (612.70 cm^{-1}) and $A_{1g}(2)$ (664.10 cm^{-1}) for Mn-Zn ferrite are consistent with earlier reported data [2]. High wavenumber bands assigned to $A_{1g}(1)$ and $A_{1g}(2)$ modes generated by the bonds in (Fe^{3+}) O_6 octahedron. The doublet like feature in Mn-Zn nano ferrites is attributed to the local cation distribution. Quite generally, the Raman shift might be due to different calcinations temperatures, vacancies, lattice strain, stoichiometry loss, structural imperfections and reduced size to quantized lattice vibrations.

The variations of frequency dependence real part of dielectric permittivity (ε') and dielectric loss ($\tan\delta$) at different temperature for Mn-Zn nano ferrites are shown in Fig. 3 and 4. It has been observed that nano ferrites decrease in dielectric constant (ε') and loss ($\tan\delta$) as the frequency increases from 100 Hz to 10 MHz. The dielectric response and loss behavior of Mn-Zn nano ferrite at 300 and 373 K are clearly shown in inset of Fig. 3 and 4. Low temperature fired Mn-Zn nano ferrite documents a decreasing trend in ε' and $\tan\delta$ with increasing frequency and almost approach frequency independent behavior in higher frequency region (~ 1 MHz). The above variation of dielectric constant can be understood on the basis of interfacial space charge relaxation [9].

Dielectric constant and loss tangent enhances with increase of different temperature and is due to the fact that hopping of charge carrier is thermally activated $Fe^{3+} \leftrightarrow Fe^{2+}$ and $Mn^{2+} \leftrightarrow Mn^{3+}$ dipoles responsible for the relaxation process with increase of temperature causing the increase of dielectric polarization and henceforth both ε' and $\tan\delta$ increases. The changes in the dielectric loss with frequency at a different temperature represent a peaking behavior as shown in the inset of Fig. 4. The peak is attributed to the resonance effect arise due to the matching of the time period of the applied electric field with those of the corresponding relaxation phenomena [10]. The value of the loss tangent is ~ 0.08 for Mn-Zn nano ferrites measured at high frequency 10 MHz (300 K) comparable with earlier measured value of $MnFe_2O_4$ [11]. We thus comment that the nano sized Mn-Zn ferrites are better in high frequency device application because of low dielectric loss.

The variation of *ac* conductivity with frequency observed at different temperature is shown in Fig. 5. All the curves exhibit the significant dispersion with frequency, which is an important behavior of ferrites. The *ac* conductivity gradually increases as the frequency of applied field increases and is explained on the basis of the hopping charge mechanism. At low frequency, the *ac* conductivity is frequency independent due to the fact that the grain boundaries are more effective than grains in electrical conduction process. Thus, the hopping of Fe^{2+} and Fe^{3+} ions are bound at lower frequencies. Further amplification of frequency, conductive grains become more active and promote the conduction mechanism. Another factor that influences the electrical conductivity of the ferrites is the hopping length (L_A and L_B) of the charge carrier. Hence, the present result on Mn-Zn nano ferrites shows that *ac* conductivity is highest [~ 0.108 S/m (573 K)] at high frequency (10 MHz). We note that nanosized Mn-Zn ferrites are better conducting material as compared to $MnFe_2O_4$.

Fig. 6 represents variation of *ac* conductivity ($\ln \sigma_{ac}$) with inverse temperature ($1/T$) at frequencies 100 Hz and 1 MHz of Mn-Zn nano ferrites. Variation of *ac* conductivity with inverse temperature supports the thermally activated transport properties. The value of activation energy (E_a) obtained from the slope is about 0.61 eV (100 Hz) and 0.41 eV (1 MHz). Lower activation energy at high frequency (~ 1 MHz) is observed as compared to that of the low frequency (100 Hz). It is noticed that at low frequencies the overall conductivity is the result of hopping of charge carriers over a

large distance and at higher frequencies is restricted to only nearest neighboring defects sites. In this case smaller response time is available to respond in the external field. The activation energy reduced with the doping Zn^{2+} ions in $MnFe_2O_4$ consistent with earlier data [12]. We end up by commenting that lower activation energy or higher conductivity makes Mn-Zn nano ferrites more useful for high frequency application.

Cole – Cole plots of imaginary (reactive) part (M'') of electric modulus of Mn-Zn nano ferrites at different temperature (300 – 573 K) are shown in Fig. 7. No complete semicircles or arcs have been observed. At room temperature two distinct semicircular relaxations were detected. The arc on the left (high frequency) is referring to the electrical response within the grain interior while the response on the right (low frequency) infers to the grain boundaries [13]. As the temperature enhances (473 – 573 K), the diameter of the incomplete arc reduced indicating a reduction of the grain interior resistance.

4 Conclusions

In summary, Mn-Zn nano ferrites were successfully prepared by low temperature fired sol-gel auto combustion method and was further investigated by lab and Synchrotron x-ray diffraction, Raman scattering and temperature dependent dielectric measurements. X-ray powder diffraction confirms that mixed ferrites form face centred cubic structure with F*d*3*m* space group and appearance of secondary phase of α-Fe_2O_3 in Mn-Zn nano ferrite. Room temperature active phonon mode also indicates the spinel nature. The real part of dielectric permittivity (ε') with frequency was observed and successfully explained on the basis of hopping mechanism. Reduced dielectric loss (0.08) at high frequency 10 MHz (300 K) for Mn-Zn nano ferrites makes them suitable material for high frequency devices and technological application. The observed *ac* conductivity is appropriate in charge carriers between Fe^{2+} and Fe^{3+} ions. Activation energy is observed to be lower at high frequency (1 MHz). Cole – Cole plot of electric modulus signifying the electrical conduction process.

Acknowledgments

UGC-DAE-CSR, as an institute is acknowledged for extending its facilities. The authors acknowledge Dr. M. Gupta, Dr. V. G. Sathe, and Dr. V. Ganesan of UGC-DAE CSR, Indore for fruitful discussions. Financial support from UGC-DAE CSR (Grant No.: CSR IC/BL- 22/CRS- 119- 2014/269), Indore is gratefully acknowledged.

References

[1] L. Nilar, M. A. N. Fauzi, S. Sreekantan and R. Othman, *Physica B.* 461, 134 **(2015)**.
[2] D. Varshney, K. Verma and A. Kumar, *Mat. Chem. and Phys*. 131, 413 **(2011)**.
[3] G. A. Petitt and D. W. Forester, *Phys. Rev. B*. 4, 3912 **(1971)**.
[4] M. A. Rehman and G. Asghar, *J. Alloys Compd*. 509, 435 **(2011)**.
[5] L. Nilar, R. Othman, M. A. N. Fauzi, S. Sreekantan, T. C. Yong, R. Singh and C. C. Tin, *Mat.Char*. 110, 109 **(2015)**.
[6] W. Wang, C. Zang and Q. Jiao, *J. Magn. Magn. Mater*. 349, 116 **(2014)**.
[7] A. K. M. Zakaria, M. A. Asgar, F. U. Ahmed, A. K. Azad, S. M. Yunus, S. K. Paranjpe and A. Das, *Ind. J. Pure Appl. Phys*. 40, 46 **(2002)**.
[8] B. D. Hosterman, J. W. Farley and A. L. Johnson, *J. Phys. Chem. Solids* 74, 985 **(2013)**.
[9] E. V. Gopalan, K. A. Malini, S. Saravanan, D. S. Kumar, Y. Yoshida and M. R. Anantharama, *J. Phys. D: Appl. Phys*. 41, 185005 **(2008)**.
[10] K. Verma, A. Kumar and D. Varshney, *J. Alloys Compd*. 526, 91 **(2012)**.
[11] M. J. Akhtar and M. Younas, *Solid Sta. Sci*. 14, 1536 **(2012)**.
[12] S. A. Mazen, A. E. Rahiem and B. A. Sabrah, *J. Mat. Sci*. 22, 4177 **(1987)**.
[13] H. Ye, R. B Jackman and P. Hing, *J. Appl. Phys*. 94, 12 **(2003)**.

Figure captions

Fig. 1 Synchrotron and lab x-ray diffraction of Mn-Zn ferrites.
Fig. 2 Room temperature Raman spectra of Mn-Zn ferrites.
Fig. 3 Dielectric constant (ε') of Mn-Zn ferrites at different temperatures.
Fig. 4 Dielectric loss (tanδ) of Mn-Zn ferrites at different temperatures.
Fig. 5 Frequency dependence *ac* conductivity (σ_{ac}) of Mn-Zn ferrites at different temperatures.
Fig. 6 Variation of ln σ_{ac} with temperature for Mn-Zn ferrites.
Fig. 7 Cole – Cole plots of electric modulus for Mn-Zn ferrites.

Structural and electrical properties of low temperature fire Mn-Zn nano ferrite for high frequency application
Pankaj Choudhary*

Fig. 1

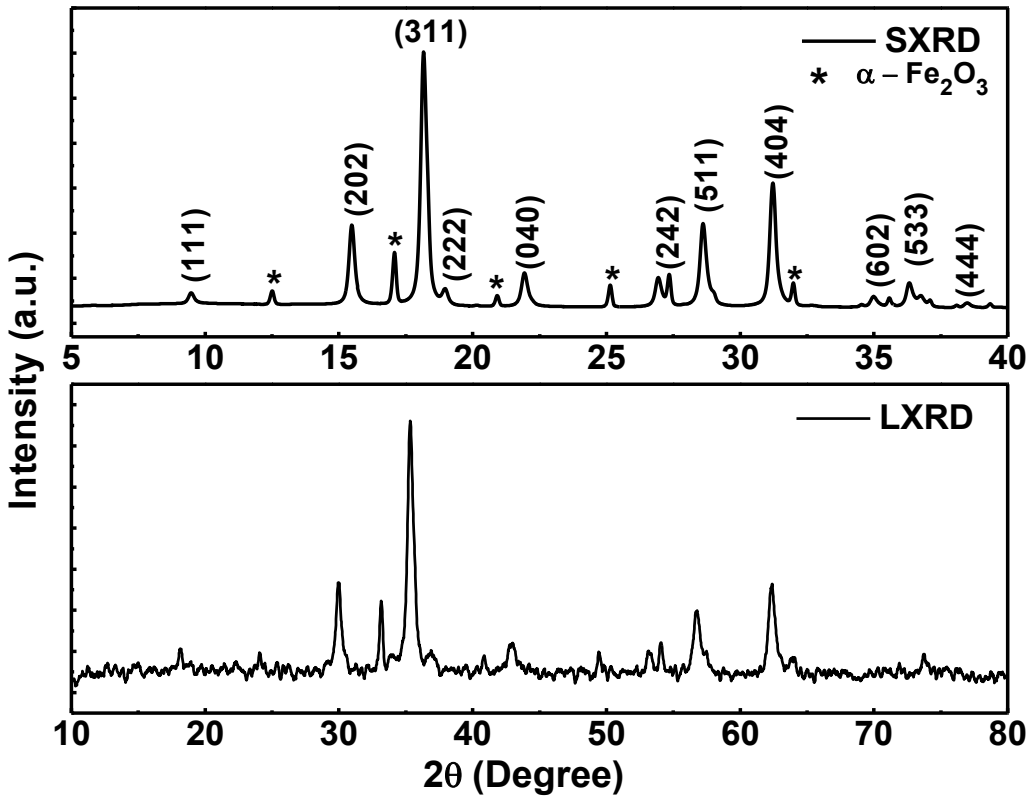

Structural and electrical properties of low temperature fire Mn-Zn nano ferrite for high frequency application
Pankaj Choudhary*

Fig. 2 (Color)

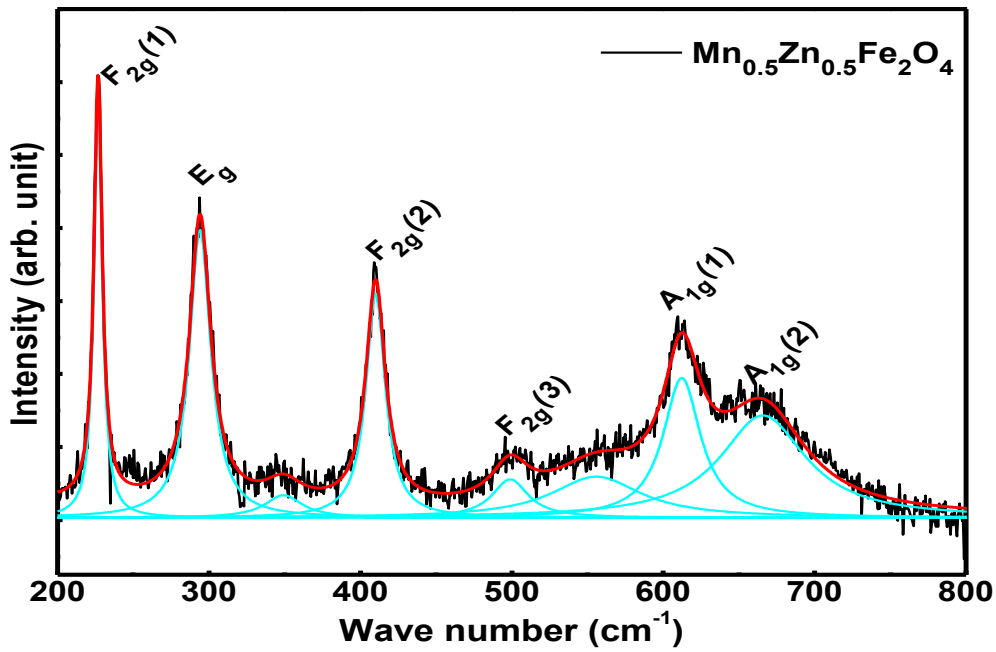

Structural and electrical properties of low temperature fire Mn-Zn nano ferrite for high frequency application
Pankaj Choudhary*

Fig. 3 (Color)

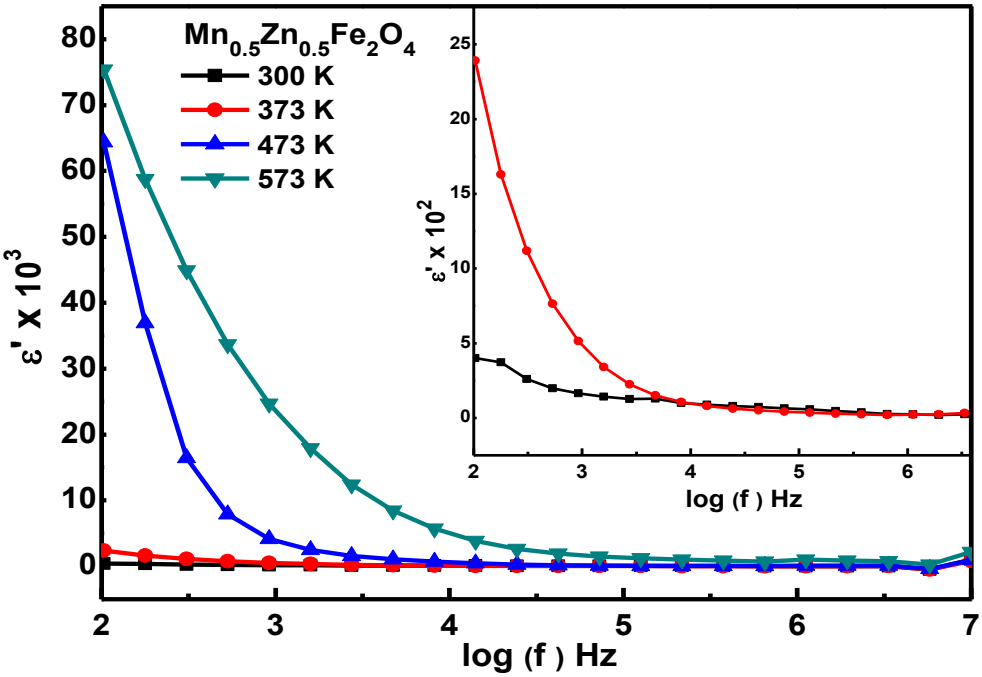

Structural and electrical properties of low temperature fire Mn-Zn nano ferrite for high frequency application
Pankaj Choudhary*

Fig. 4 (Color)

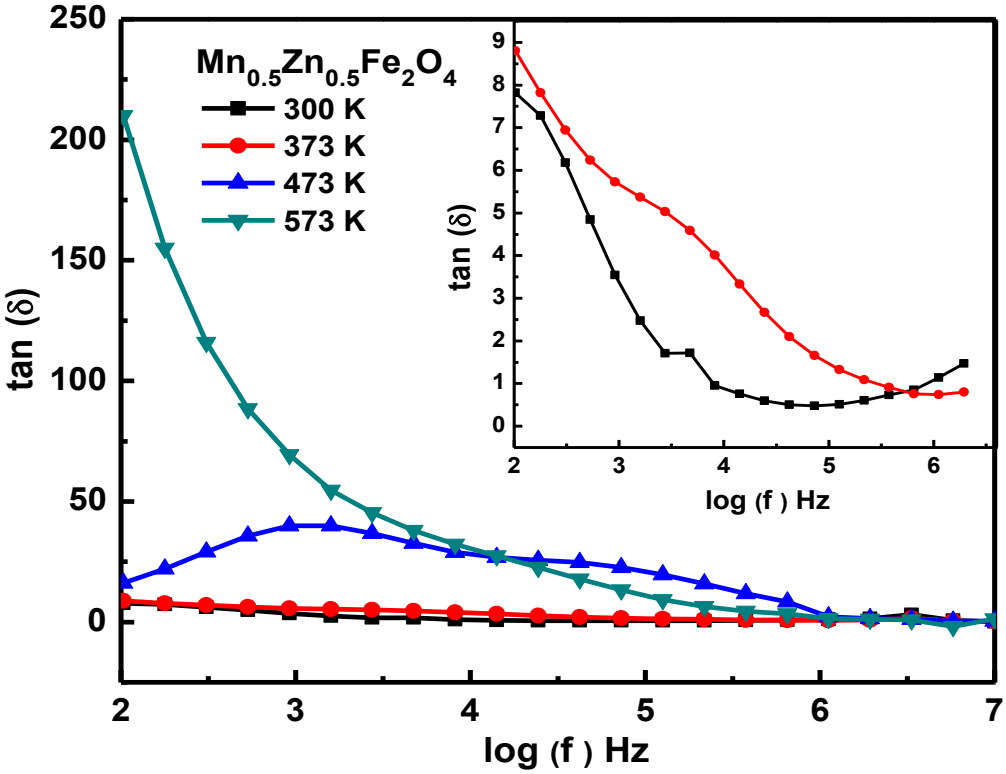

Structural and electrical properties of low temperature fire Mn-Zn nano ferrite for high frequency application
Pankaj Choudhary*

Fig. 5 (Color)

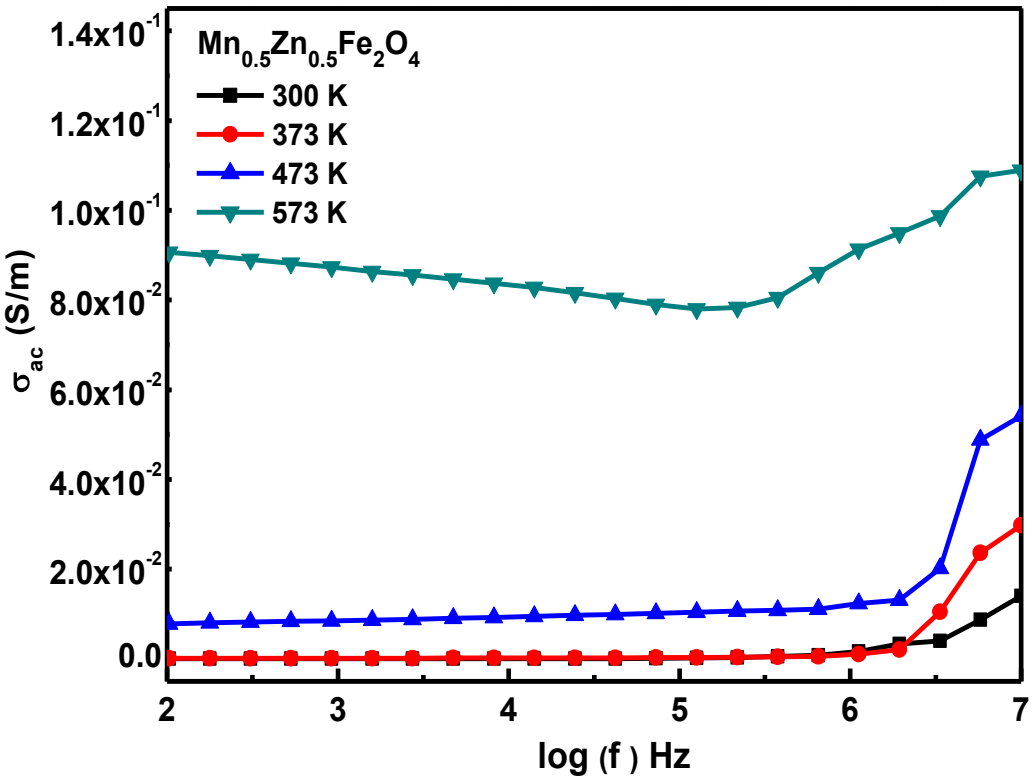

Structural and electrical properties of low temperature fire Mn-Zn nano ferrite for high frequency application
Pankaj Choudhary*

Fig. 6 (Color)

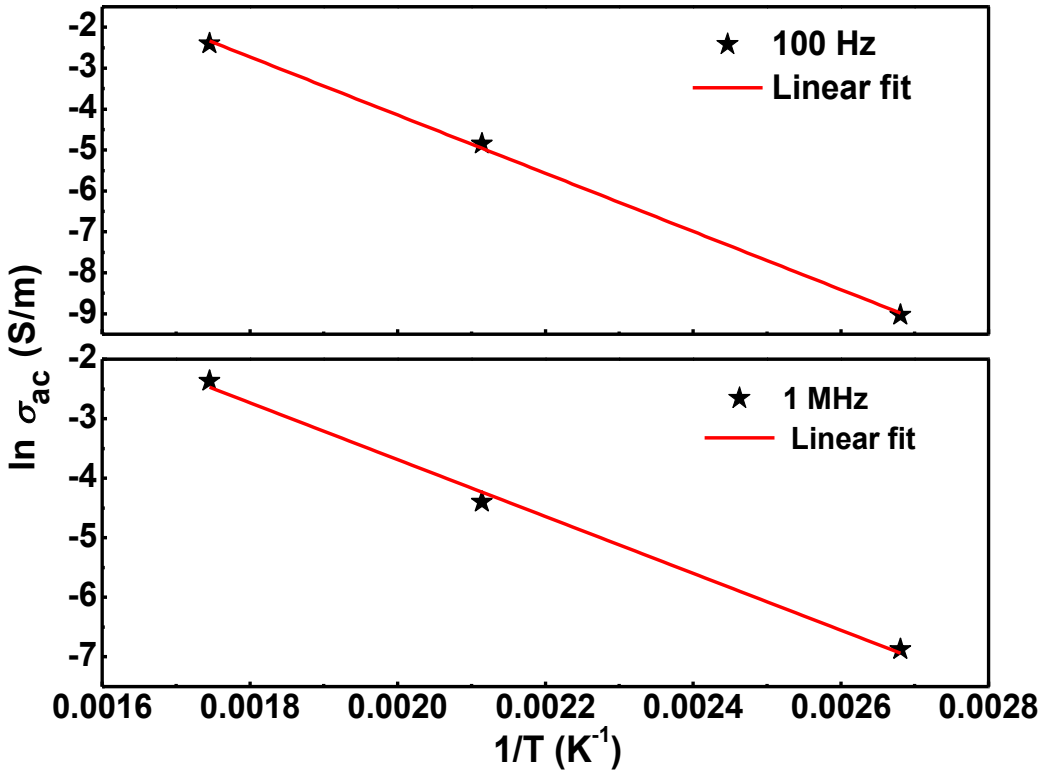

Structural and electrical properties of low temperature fire Mn-Zn nano ferrite for high frequency application
Pankaj Choudhary*

Fig. 7 (Color)

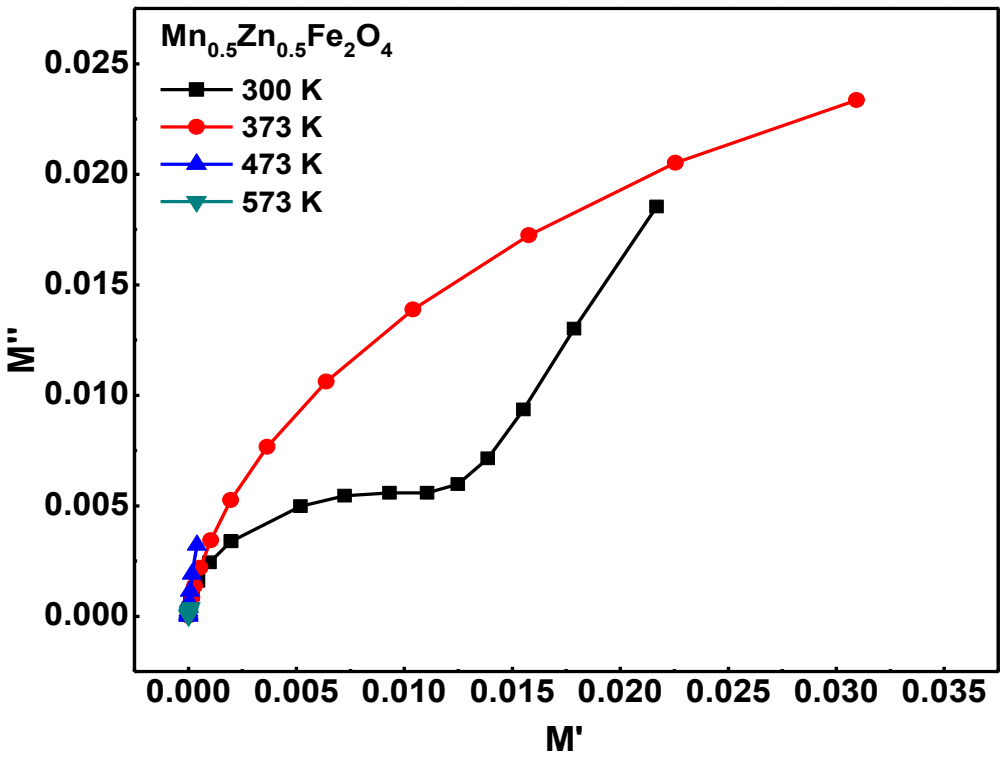

Structural and electrical properties of low temperature fire Mn-Zn nano ferrite for high frequency application
Pankaj Choudhary*

Table 1: Particle size (D), lattice constant (a), x-ray density (ρ_x), tetrahedral and octahedral hopping length (L_A and L_B), micro strain (ε) and dislocation density (δ) of synthesized Mn-Zn nano ferrite.

	D (nm)	a (Å)	ρ_x (g/cm^3)	L_A (Å)	L_B (Å)	ε	$\delta \times 10^{14}$ (1/m^2)
Lab XRD	16.0 ± 0.001	8.410 (3)	5.267	3.64	2.97	0.423	3.88
Synchrotron XRD	15.4 ± 0.0001	8.441 (4)	5.209	3.65	2.98	0.443	4.17

